

Temperature-dependent midinfrared photoluminescence of epitaxial PbTe/CdTe quantum dots and calculation of the corresponding transition energy

T. Schwarzl,^{1,*} E. Kaufmann,¹ G. Springholz,¹ K. Koike,² T. Hotei,² M. Yano,² and W. Heiss¹

¹*Institut für Halbleiter- und Festkörperphysik, Johannes Kepler Universität Linz, Altenbergerstraße 69, A-4040 Linz, Austria*

²*Osaka Institute of Technology, Asahi-ku Ohmiya, Osaka 535-8585, Japan*

(Received 10 July 2008; published 23 October 2008)

We present the temperature dependence of continuous-wave midinfrared photoluminescence of PbTe quantum dots in a CdTe matrix. The quantum dots are formed by epitaxial precipitation of a two-dimensional PbTe layer upon thermal annealing. A strong shift of the emission to longer wavelengths with decreasing temperature is found. This shift is not only caused by the strong temperature dependence of the band gap of PbTe but also by the strain in the dot as well as by the change in quantization energies, both being temperature dependent due to the thermal-expansion mismatch between PbTe and CdTe, and via the effective masses of PbTe. At low temperatures we observed an increase in the emission intensity with rising temperature, depending on dot size. This is attributed to the presence of a dark ground state, as was also observed for lead salt nanocrystals. The influence of the excitation power on the emission spectra at various temperatures indicates carrier redistribution between the dots. Furthermore, an analytical calculation of the ground-state transition energy in the dots is performed using a spherical dot shape, and including the temperature-dependent strain in the dots and the matrix as well as the temperature dependence of the effective masses of PbTe. From these model calculations, a good agreement to the experimental data is obtained over the whole temperature range from 20 to 300 K.

DOI: [10.1103/PhysRevB.78.165320](https://doi.org/10.1103/PhysRevB.78.165320)

PACS number(s): 78.67.Hc, 81.07.Ta, 78.55.Hx, 78.55.Et

I. INTRODUCTION

In recent years, a lot of effort has been devoted to the investigation of semiconductor systems with reduced dimensionality. In particular, reducing the dimensionality to zero so that free carriers are confined in all three directions of space results in an atomlike density of states.¹⁻³ In such quantum dots (QDs), not only interesting physical effects were observed but also applications for optical devices, such as low-threshold semiconductor lasers, have been shown.⁴⁻⁷ The most common fabrication method for QDs is the Stranski-Krastanow (SK) growth mode of strained-layer heteroepitaxy, which yields defect-free QDs (Ref. 8) exhibiting strong photoluminescence (PL) emission. SK dots usually exhibit relatively flat dot shapes and are connected by a two-dimensional wetting layer on which the dots are formed.

The typical and most studied materials for SK dots are In(Ga)As/GaAs, leading to emission between 1 and 1.3 μm . The temperature dependence of the PL of these QDs was studied in some detail. In particular, the integrated PL intensity, the peak position, and the widths of the PL emission show a behavior not observed in quantum well systems. The PL intensity of QDs usually remains constant at low temperatures but starts to decrease slowly at intermediate temperatures (about 50–120 K) and finally decreases exponentially for higher temperatures.⁹⁻¹¹ The peak energy exhibits sometimes a redshift with almost sigmoidal form with increasing temperature, which is larger than the band-gap change of the dots with temperature.¹¹ However, for InGaAs/GaAs QDs produced by droplet epitaxy without a wetting layer,¹² this shift follows the temperature-dependent band gap of the dot.¹³ Also the width of the emission narrows with rising temperature at intermediate temperatures,⁹ an effect that vanishes again for the dots without a wetting layer.¹³ The commonly accepted explanation for these observations is the

thermally driven carrier redistribution between the dots and carrier evaporation out of the dots.

It is interesting to see if such effects are also present in other QD systems emitting at longer wavelengths, in particular in the midinfrared (MIR) range that is technologically important for gas sensing applications. Although recently InSb/GaSb SK dots with PL emission around 3.5 μm at room temperature were shown,¹⁴ the lead salt (IV-VI) materials are commonly used for such MIR applications.¹⁵⁻¹⁸ Beside their narrow-band gap, the IV-VI compounds have the advantages of nearly symmetric conduction and valence bands at the direct band gap, and of low Auger recombination rates.¹⁹ Furthermore, PbTe exhibits very large electron and hole Bohr radii a_B of 360 and 290 nm at 300 K, respectively, due to its large dielectric constant ($\epsilon_s=414$ at 300 K) (Ref. 20) and small effective masses.²¹ Thus, the strong confinement limit is easily reached even for larger dot sizes. Lead salt QDs have mostly been fabricated as colloidal nanocrystals in liquid solutions giving strong and tunable PL emission between 1 and 4 μm .²²⁻²⁴ Also molecular-beam epitaxy (MBE) grown SK PbSe/PbEuTe QDs were successfully demonstrated.^{25,26} For these types of dots, however, photocurrent spectroscopy studies in the MIR indicate a strain-induced type-II band alignment²⁷ leading to poor PL emission efficiency.

Recently, we presented an approach for fabrication of high-quality lead salt QDs for the MIR based on the epitaxial precipitation of lattice-type mismatched heterostructures.²⁸ This approach results in wetting-layer-free QDs with highly symmetric shapes^{28,29} and atomically sharp heterointerfaces.²⁹⁻³¹ Furthermore, these QDs are defect free and exhibit an intense continuous-wave (cw) PL at room temperature.^{28,29} We are also able to control the dot sizes and the vertical positions of the dots by the growth conditions.³² The employed semiconductors are PbTe with a rock-salt lat-

tice as dot material and CdTe with a zinc-blende lattice as matrix material. This material combination exhibits only a small lattice mismatch of 0.29% at room temperature. The fabrication starts with MBE growth of a two-dimensional PbTe layer ($E_g=320$ meV at 300 K) (Ref. 33) with a thickness in the nanometer range sandwiched between CdTe barrier layers ($E_g=1.53$ eV).³⁴ This PbTe quantum well is subsequently transformed into QDs by thermal annealing, based on the immiscibility of the two materials³⁵ and the minimization of the interface energy. Also PbSnTe QDs in CdTe with Sn contents up to 20% have been fabricated in a similar way.³⁶ First, results on the temperature-dependent PL of PbTe and PnSnTe dots have showed a strong shift of the peak accompanied by an unusual change in intensity.³⁷

In the current work, we present a detailed study of the temperature dependence of the cw PL of PbTe/CdTe QDs for different dot sizes. Interestingly, we observe an increase in the PL intensity with rising temperature before it starts to decrease above a certain temperature, and the temperature with maximum PL output depends on the size of the dots. We suggest that this behavior arises from the splitting of the ground state into a bright state and a lower lying dark state, as was also observed in nanocrystal quantum dots. In addition, the excitation power dependence of the PL spectra at various temperatures is analyzed and attributed to carrier redistribution between the dots over the barrier. In the second part of the paper, we explain the strong temperature shift of the PL peak by means of a calculation of the transition energy responsible for the PL emission. This shift and its origin are completely different as compared to those of III-V dots. For the analytical calculation, we make use of the fact that the ground-state transition in a spherical dot with finite barrier heights can be calculated in analogy to the first-excited state in a quantum well with the same dimensions (see, e.g., Ref. 38). We also include the strain in the dots and the anisotropic effective masses of PbTe, both being temperature dependent, and we obtain a good agreement with the experimental data.

II. SAMPLE STRUCTURE AND EXPERIMENTAL DETAILS

The samples were grown by MBE using solid source CdTe, PbTe, Cd, and Te effusion cells on semi-insulating (100)-oriented GaAs substrates. High quality CdTe/MnTe buffer layers were grown as described in detail in Ref. 39. This is necessary because of the large difference in lattice constant between GaAs and CdTe. First, a 80-nm-thick CdTe film was grown at 280 °C on a sulfur-treated (100)-oriented GaAs substrate as a nucleation layer for (100)-oriented CdTe growth, and then a 400-nm-thick CdTe film was grown at 320 °C. This two-step growth was effective in obtaining a smooth (100)-oriented CdTe surface on the GaAs substrates. Subsequently, an *in situ* thermal annealing at 380 °C for 30 min was performed after capping the CdTe surface with a 100-nm-thick MnTe layer. This MnTe capping was employed to suppress the reevaporation of CdTe during annealing.³⁹ Onto the MnTe/CdTe buffer layer, 50 nm CdTe and then a 25-period (5 nm MnTe)/(2 nm CdTe) strained-layer superlat-

tice (SLS) was grown at 280 °C to reduce the strain induced by the MnTe layer, and then a 600-nm-thick CdTe layer at 320 °C was deposited. The quality of the uppermost CdTe layer on the SLS was very high as evidenced by atomic force microscopy (AFM) with an average roughness below 0.5 nm, and PL spectra consisting only of strong CdTe band-gap emission and no defect-related PL peaks, which were present in samples without the SLS.³⁹ On the Cd-terminated CdTe buffer, PbTe layers with different thicknesses of 3 and 5 nm were deposited using a low growth temperature of 220 °C to ensure a two-dimensional growth without island formation, as proven by *in situ* reflection high-energy electron diffraction (RHEED) and AFM.⁴⁰ Finally, a 50 nm CdTe barrier layer was grown on top to form a PbTe quantum well and a 25 nm MnTe cap layer to finish the layer sequence. The growth rate was 100 nm/h for all layers and the whole growth process was monitored by *in situ* RHEED.

By postgrowth thermal annealing in inert N₂ atmosphere, the PbTe quantum well layers are transformed into isolated quantum dot nanoprecipitates^{28,29} due to the immiscibility of PbTe and CdTe.³⁵ The annealing conditions (duration and temperature) were optimized for each sample to achieve the highest cw-PL intensity at room temperature. These conditions were 320 °C for 10 min and 350 °C for 10 min for the 3 and 5 nm PbTe sample, respectively. According to our recent transmission electron microscopy (TEM) studies,³² for these PbTe thicknesses PbTe dots with diameters between about 20 and 30 nm are obtained. These comparatively large dot sizes have the advantage that possible interface states do not significantly affect the electronic properties of the dots. Due to very large electron and hole Bohr radii of PbTe, strong confinement is easily reached even for these dot sizes. As shown by TEM,^{28,29,32} the annealed dots have a centrosymmetric shape of a small-rhombo-cubo-octahedron which is the dot shape in thermal equilibrium (minimization of interface energies).²⁸ The shape resembles a faceted sphere, as was also observed for colloidal PbSe nanocrystals in liquid solutions.⁴¹ From the TEM investigations, we also know that the dots are essentially defect free and exhibit atomically sharp heterointerfaces.²⁸⁻³¹

The PL measurements were done with a cw diode laser with a wavelength of 1480 nm and an output power of up to 245 mW. The pump laser was focused on the sample placed in a He flow cryostat with a spot size of about 0.1 mm² under an angle of 45° and the PL emission was recorded by lock-in technique with a liquid-nitrogen-cooled InSb infrared detector mounted on a grating spectrometer.

III. EXPERIMENTAL RESULTS AND DISCUSSION

A. Temperature dependence of the photoluminescence spectra

Figure 1 shows the cw-PL spectra for the two QD samples with initial 3 and 5 nm PbTe layers for temperatures between 20 and 300 K. For all temperatures and both samples, there is only a single PL peak with a Gaussian line shape and a linewidth between 330 and 460 nm. The absence of an additional PL peak from residuals of the quantum well (as seen in Ref. 28) shows that the PbTe quantum well layers were completely transformed into PbTe QDs by the optimized thermal

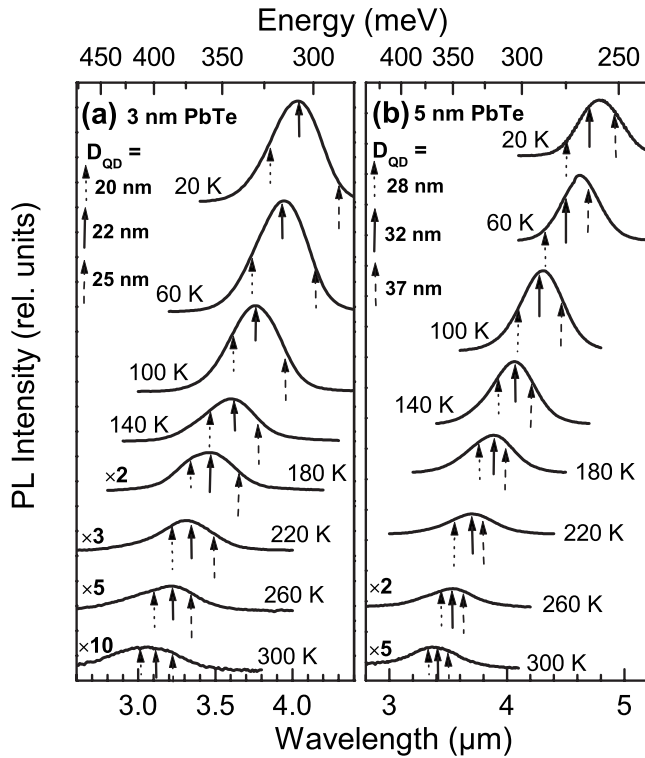


FIG. 1. Temperature-dependent continuous-wave PL spectra for PbTe/CdTe quantum dots formed from initially (a) a 3-nm-thick and (b) a 5-nm-thick PbTe layer. The arrows depict the calculated ground-state transition energy for different dot diameters D_{QD} as indicated.

annealing process. As shown in Fig. 1, with decreasing temperature the PL peak strongly shifts to longer wavelengths. For the 3 nm sample, the emission shifts from 3 (406 meV) to $4 \mu\text{m}$ (308 meV) between 300 and 20 K. A slightly larger shift is found for the 5 nm sample from 3.4 (368 meV) to $4.8 \mu\text{m}$ (258 meV) in the same temperature range.

This shift is also shown in Fig. 2, in which the energy of the PL maxima of the spectra is plotted as a function of the temperature (symbols). These experimental data are compared to the band gap of bulk PbTe (Ref. 33) (dash-dotted line) revealing immediately that (1) most of the shift with temperature arises from the strong *positive* temperature dependence of the band gap of PbTe ($dE_g/dT = +0.44 \text{ meV/K}$), which is an anomaly common to all lead salts,⁴² and (2) the increase in the transition energy due to the confinement in the dots. However, it is seen that the temperature shift of the QD PL is slightly smaller (0.36 and 0.39 meV/K for the 3 and 5 nm samples, respectively) than for bulk PbTe. The reason for this is, on the one hand, the strain in the dots due to the small lattice mismatch between PbTe and CdTe, and on the other hand, the confinement energy into which a considerable temperature dependence enters through the PbTe effective masses. The details of these considerations will be presented in Sec. IV, which deals with calculation of the ground-state transition energy responsible for the PL peak position. By comparing the results of the two samples in Fig. 2 one also sees that the confinement is much larger for the originally 3-nm-thick layer than for the 5 nm

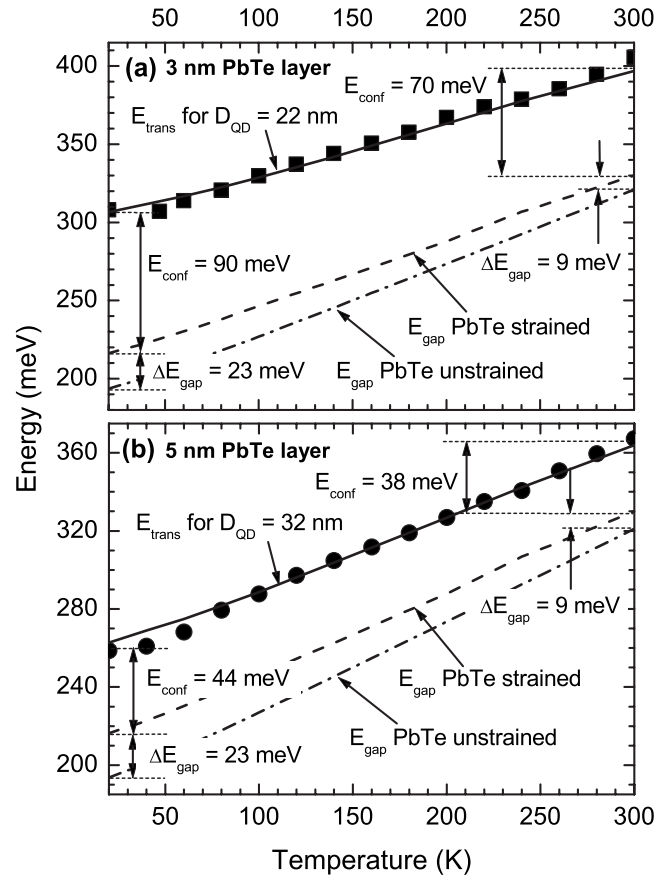


FIG. 2. Peak energy of the PL emission spectra of PbTe/CdTe dots from Fig. 1 as a function of temperature (symbols) for (a) 3 and (b) 5 nm PbTe. The full, dashed, and dash-dotted lines depict the calculation of the ground-state transition energy for (a) 22 and (b) 32 nm dot diameters, the band gap of isotropically strained PbTe, and the band gap of bulk PbTe, respectively. The confinement energy E_{conf} and the energy change of the band gap of PbTe due to the isotropic strain correction ΔE_{gap} is indicated for 300 and 20 K.

layer, which indicates a larger dot size for the 5 nm PbTe layer. An anomaly in the PL peak shift with an almost sigmoidal form larger than the band-gap change as observed in most III-V dots¹¹ was not found here. This behavior is usually caused by thermally activated carrier transfer between the dots via the wetting layer, and is absent for wetting-layer-free III-V dots.¹³ In our wetting-layer-free dots, however, there are other indications for carrier transfer, as will be outlined in Sec. III B.

The integrated PL intensity of both samples is depicted in Fig. 3 as a function of temperature between 20 and 300 K. Starting from 20 K, surprisingly the PL intensity increases at first until a certain temperature is reached above which the PL intensity decreases considerably. The temperature with the maximum PL output is about 55 and 100 K for the 3 and the 5 nm samples, respectively (dotted lines in Fig. 3). The low-temperature behavior is in contrast to what has been observed for III-V dots for which the intensity is constant in this range. At higher temperatures III-V dots show an almost exponential decrease in the intensity due to the thermal escape of carriers out of the dots.⁹⁻¹¹ This thermal quenching can be fitted with an $\exp(E_a/kT)$ behavior with an activation

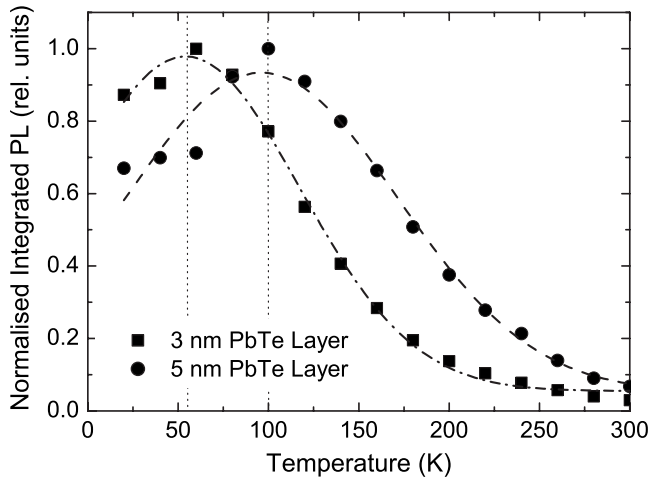


FIG. 3. Normalized integrated PL intensity vs temperature for PbTe/CdTe dots with a 3-nm-thick (squares) and a 5-nm-thick PbTe layer (circles). The lines are guides to the eye.

energy E_a which matches the barrier height of either one or both types of carriers.¹⁰ Although the quenching with higher temperatures is much smaller in our case (only about a factor of 10, as compared to 2–3 orders of magnitude for III-V SK dots),^{9–11} it still can roughly be fitted with an exponential function resulting in an activation energy of 50–100 meV. This small activation energy is an indication that the band offsets for PbTe/CdTe are rather asymmetric with a ratio of about 1:10, leading to a small barrier height for one type of carrier. The considerably smaller thermal quenching of the PL intensity as compared to most III-V dots is a consequence of the absence of a wetting layer in our dots, which would provide an efficient channel for the loss of carriers due to nonradiative recombination.¹³

A possible reason for the uncommon behavior at low temperatures is the presence of a dark ground state, as was also experimentally shown for IV-VI nanocrystal QDs in silicate glass.⁴³ In this case, the ground-state transition is splitted into two states, one with a short lifetime (bright state) and one with a long lifetime (dark state) lying energetically below the short-lived one (see also calculation in Ref. 44). At low temperatures only the lower-energy dark state is occupied leading to reduced emission intensity. By increasing the temperature the higher-energy bright state will be thermally filled and the intensity increases. We experimentally observe that for the 5 nm sample with larger dots the PL intensity decrease at low temperatures is larger than for the 3 nm sample, and that one needs also a higher temperature to thermally occupy the bright state and reach the maximum PL output, thus indicating a larger splitting for larger dots. However, this is in contrast to a calculation of this exchange splitting of the ground state for colloidal PbSe QDs with diameters of 3 and 6 nm (Ref. 44) that showed a decreasing splitting with increasing dot size. This disagreement indicates either a different behavior for our much larger dots or another additional fact that influences the temperature dependence of the emission intensity of our PbTe/CdTe dots.

Also a type-I/type-II band alignment transition with decreasing temperature could explain the lower emission inten-

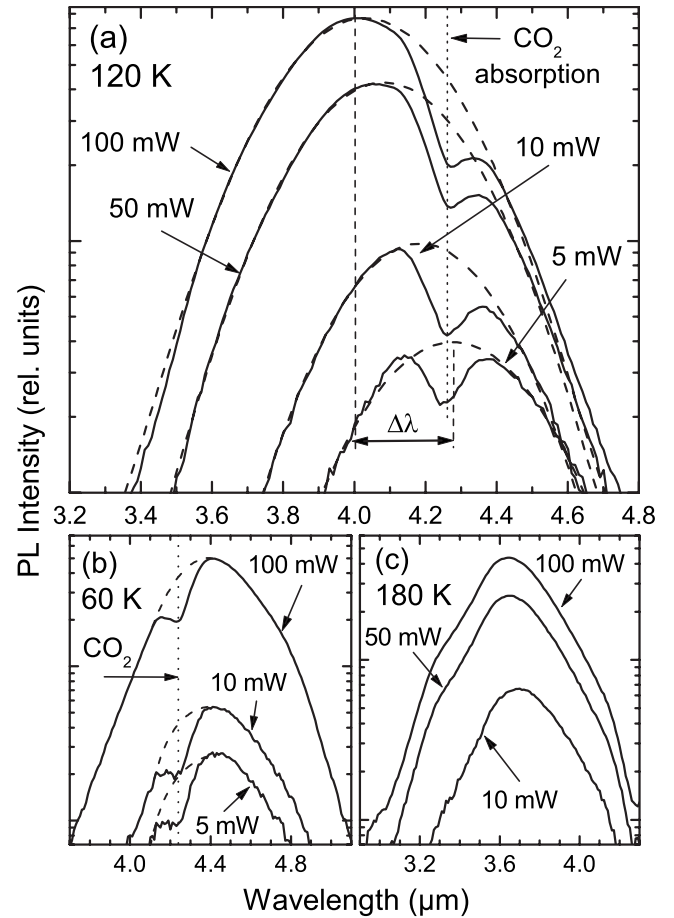


FIG. 4. Excitation power dependent PL spectra of PbTe/CdTe dots with 5 nm PbTe at different temperatures of (a) 120, (b) 60, and (c) 180 K on a logarithmic scale. The dips at $4.25 \mu\text{m}$ indicated by the dotted line arise from residual CO_2 absorption in the optical measurement path. The dashed lines are Gaussian line fits to the data.

sity at lower temperatures, as was suggested in Ref. 37. However, the possible origin for type-II band alignment at low temperatures—the increasing strain in the dots—is overestimated in Ref. 37 because the matrix was treated as inelastic medium and thus unstrained (for details on effect of strain on the transition energy of the dots, see Sec. IV A). Furthermore, for a type-II alignment the emission intensity should be very small, which is not the case in the experimental results. Therefore, a change in band alignment—also arising from other effects than strain—can rather be ruled out.

B. Pump power dependence of the photoluminescence spectra

To complete the PL emission studies of the PbTe/CdTe QDs, the pump power dependence of the PL spectra was measured at different temperatures. As shown in Fig. 4, a different behavior at the various temperatures was found. Whereas at 120 K [Fig. 4(a)] a pronounced redshift of 280 nm with decreasing excitation power from 100 to 5 mW is found [labeled $\Delta\lambda$ in Fig. 4(a)], for both lower and higher temperatures no such shift was observed [see Figs. 4(b) and

4(c)]. This indicates that the observed redshift for lower powers is not due to local heating of the sample at higher pump powers, which should be independent on temperature. Also, a PbTe quantum well reference sample exhibited no shift of the PL peak with varying pump power. The dip at 4.25 μm in all spectra in Fig. 4 arises from residual CO_2 absorption in the optical measurement path. In addition, we also observed a slightly decreasing linewidth of the PL emission peak with increasing temperatures from 20 to about 120 K and a constant or increasing linewidth at higher temperatures.

We attribute the observed behavior to thermally induced carrier redistribution between individual QDs as was also reported for SK III-V dots^{9,45} as well as for CdTe/ZnTe self-assembled QDs connected by a wetting layer.⁴⁶ In the latter paper, a simple model explains the observed effect as follows: At low temperatures, at which the thermal energy of the carriers localized in the QDs is so small that they cannot escape, the initial population of the QDs determines the PL spectrum independent of the pump power. As the temperature increases, the carriers are able to escape from the dots to the wetting layer and they are redistributed to energetically favorable larger dots. This process results in a redshift of the PL emission with decreasing excitation power, as only the lowest-energy states of the whole dot ensemble are occupied and, consequently, also in a smaller linewidth as compared to the low-temperature regime. Finally, at high enough temperatures the thermally activated carriers do not have enough time to find an energetically favorite QD before they recombine nonradiatively. Thus, the emission only comes from carriers in dots in which they were initially excited, as in the low-temperature regime independent of the excitation power. This explanation also fits to the results from our dots, apart from the important fact that the PbTe dots have no wetting layer connecting the dots. And without such a layer the carrier redistribution should be inhibited, as was also shown directly in the paper on CdTe/ZnTe dots.⁴⁶ Therefore, we conclude that in the PbTe dots the carriers are allowed to redistribute through the CdTe matrix despite the high band-gap difference. This again indicates that the band offsets in conduction and valence bands are strongly different so that the thermal redistribution over the barriers is facilitated for one type of carrier.

IV. CALCULATION OF GROUND-STATE TRANSITION ENERGY

In order to correctly explain the temperature shift of the PL emission shown in Sec. III, a calculation of the ground-state transition energy responsible for the PL emission is performed. For this we make use of the fact that the ground-state energy in a spherical dot with finite barrier heights can be calculated in analogy to the first-excited state energy in a quantum well with the same dimensions (see, e.g., Ref. 38). The shape of a sphere is a good approximation to the centrosymmetric shape of the PbTe/CdTe dots corresponding to a small-rhomb-cubo-octahedron which looks like a faceted sphere.²⁸ Therefore, this approximation seems to fit better to the real shape of the dots than the model based on a quantum

box shape recently used for calculations of optical transitions in PbTe/CdTe dots.⁴⁷ We also include the strain in the dots *as well as* in the matrix due to the temperature-dependent lattice mismatch between PbTe and CdTe.^{20,34} So far this strain effect was considered for the dots only.³⁷ The change of the confinement due to the temperature dependence of the effective masses is also an important contribution. The strong effective-mass anisotropy in bulk PbTe is taken into account by spherical averaging of the effective masses for different directions in k space, which is justified by the strong confinement of the carriers in all directions in the dot (Bohr radius of both types of carriers much larger than the dot dimensions). Calculations of energy levels for spherical dots with infinite barrier heights based on the $\vec{k}\cdot\vec{p}$ method including the full band anisotropy resulted in an error of only 4% as compared to the spherically averaged solution for the ground-state transition in PbTe dots with diameters of up to 10 nm.⁴⁸

A. Band gap in an isotropically strained spherical dot

For the calculation of the transition energy in a spherical QD, it is essential to know the change of the band gap of the dot material owing to the stress in the dot, arising from the difference of the lattice constants of dot and matrix material even if this difference is rather small as for PbTe and CdTe. Here, it is essential to consider that a major part of the dot/matrix lattice mismatch is accommodated by elastic distortion of the matrix rather than the dot itself.⁴⁹ Thus, the strain in the dot is only about one third of the relative lattice mismatch $\epsilon_0 = \Delta a/a$ (depending on the elastic constants).⁴⁹

For a spherical dot and elastically isotropic materials, the contact pressure P when the dot and the matrix are brought into contact is given by⁴⁹

$$P = -\epsilon_0 \frac{1}{\frac{1 + \nu_{\text{out}}}{2E_{\text{out}}} + \frac{1 - 2\nu_{\text{in}}}{E_{\text{in}}}}, \quad (1)$$

where E and ν are Young's modulus and Poisson's ratio of the outer (matrix) and inner (dot) materials. Since PbTe as well as CdTe are rather anisotropic materials, we use the approximation of averaged elastic constants with the anisotropy factor H defined over the elastic coefficients c_{ij} by⁵⁰

$$H = 2c_{44} + c_{12} - c_{11}. \quad (2)$$

The averaged elastic constants λ (Lamé constant) and μ (shear modulus) for a cubic crystal are then⁵⁰

$$\lambda = c_{12} - (1/5)H, \quad (3)$$

$$\mu = c_{44} - (1/5)H. \quad (4)$$

Now one can calculate the averaged Young's modulus E and Poisson's ratio ν by the above formulas using the standard relationships from elasticity theory,⁵⁰

$$E = \frac{\mu(3\lambda + 2\mu)}{\lambda + \mu}, \quad (5)$$

TABLE I. Parameters used for the calculation of the contact pressure P [Eq. (1)]. The elastic moduli c_{ij} are taken from Refs. 20 and 34.

Parameters	PbTe	CdTe
c_{11} (GPa)	105.3	53.3
c_{12} (GPa)	7.0	36.5
c_{44} (GPa)	13.2	20.4
H (GPa)	-71.9	24.0
λ (GPa)	21.4	31.7
μ (GPa)	27.6	15.6
E (GPa)	67.3	41.7
ν	0.218	0.333

$$\nu = \frac{\lambda}{2(\lambda + \mu)}. \quad (6)$$

The elastic coefficients c_{ij} (Refs. 20 and 34) and averaged elastic parameters used for calculation of the contact pressure P from Eq. (1) for PbTe and CdTe are listed in Table I. It is noted that these values are only valid for 300 K. However, using values of c_{ij} for 77 K (Refs. 34 and 51) results in a relative change in P/ϵ_0 of only 0.4%. Thus, for all calculations the values listed in Table I were used.

To calculate P the temperature dependence of the lattice mismatch, $\epsilon_0(T) = \Delta a(T)/a(T)$ must be evaluated. Starting from the lattice constants of PbTe and CdTe at 300 K (6.462 and 6.481 Å, respectively,^{20,34} resulting in a ϵ_0 of 0.29%), we make use of the full temperature dependence of the linear thermal-expansion coefficients β (Refs. 20, 34, 52, and 53) ($19.8 \times 10^{-6}/\text{K}$ and $4.9 \times 10^{-6}/\text{K}$ at 300 K for PbTe and CdTe, respectively) to calculate the mismatch at lower T . Due to the large difference of the expansion coefficients, the lattice mismatch increases with decreasing T . In that way, the temperature dependence of the lattice constants is calculated to be

$$a_{\text{PbTe}}(T) = 6.371 \text{ \AA} + 0.056 \text{ \AA} \times e^{T(\text{K})/633 \text{ K}}, \quad (7)$$

$$a_{\text{CdTe}}(T) = 6.471 \text{ \AA} + 0.003 \text{ \AA} \times e^{T(\text{K})/260 \text{ K}} \quad (T > 60 \text{ K}) \quad (8)$$

resulting in the temperature-dependent lattice mismatch between PbTe and CdTe:

$$\epsilon_0(T) = 0.0075 - 1.53 \times 10^{-5} \times T(\text{K}). \quad (9)$$

At 20 K ϵ_0 gets as large as 0.72%.

It is noted that one could also use the thermal-expansion coefficient of the GaAs substrate as reference instead of CdTe if one assumes that the CdTe layer is always pseudomorphically strained. However, since the $\beta(T)$ values of GaAs and CdTe are very similar to each other,⁵²⁻⁵⁴ this yields essentially the same results.

After calculating the pressure $P(T)$ imposed on the PbTe dots as a function of temperature, the resulting change of the energy-band gap can be given by

$$\Delta E_{\text{gap}}(T) = \frac{\partial E_{\text{gap}}}{\partial p} P(T), \quad (10)$$

with the hydrostatic pressure coefficient $\partial E_{\text{gap}}/\partial p = -75 \text{ meV/GPa}$ for PbTe (Ref. 20) (considered as constant with T). At room temperature the contact pressure P on the dot is -0.12 GPa (the minus sign indicates tensile stress on the dot because the lattice constant of the matrix is larger than that of the dot), resulting in a change in the energy gap ΔE_{gap} of $+9 \text{ meV}$. This strain-induced band-gap change increases with decreasing temperature and thus becomes more important. The resulting band gap for isotropically strained PbTe in CdTe is plotted in Fig. 2 as dashed line as a function of temperature. One can see that at 20 K this strain correction becomes as large as $+23 \text{ meV}$.

It is noted that the strain correction for the band gap for a biaxially strained PbTe quantum well in CdTe is much larger because the lattice mismatch ϵ_0 directly leads to a corresponding strain in the two-dimensional pseudomorphic epilayer in contrast to the strain in the dot which is only about one third of ϵ_0 (Ref. 49) (see text in the beginning of this section). Consequently, at 300 K the quantum well strain correction is already 21 meV and increases to 51 meV at 20 K.

B. Ground-state energy in a spherical dot with finite barriers

As mentioned above, we calculate the ground-state energy E of a spherical dot with finite barrier height V in analogy to the first-excited state (first odd solution) of a quantum well with finite barriers, setting the well width L equal to the dot diameter D (see, e.g., Ref. 38). Thus, we determine the first solution of the following equation:

$$\cot \frac{k(E) \cdot D}{2} + \frac{m_{\text{dot}}}{m_{\text{matrix}}} \left[\frac{\kappa(E)}{k(E)} + \frac{2}{k(E) \cdot D} \right] - \frac{2}{k(E) \cdot D} = 0, \quad (11)$$

with

$$k(E) = \sqrt{\frac{2m_{\text{dot}}E}{\hbar^2}}, \quad (12)$$

$$\kappa(E) = \sqrt{\frac{2m_{\text{matrix}}(V-E)}{\hbar^2}}. \quad (13)$$

The main parameters for the calculation of the energy level E_i apart from the dot size D are the effective electron and hole masses within the PbTe dot m_{dot} and the CdTe matrix m_{matrix} which are strongly temperature dependent, in particular the one for PbTe for which Ref. 21 gives detailed temperature-dependent data. The masses for PbTe decrease with temperature due to the decreasing band gap (e.g., $m_{e,t}(300 \text{ K}) = 0.031m_0$, $m_{e,t}(80 \text{ K}) = 0.024m_0$, $m_{h,t}(300 \text{ K}) = 0.036m_0$, and $m_{h,t}(80 \text{ K}) = 0.027m_0$). As a consequence, the quantum confinement for both types of carriers exhibiting similar effective masses (in contrast to most other semiconductors) will strongly increase with decreasing temperature. The masses for CdTe for 300 and 4 K are taken from Ref. 34

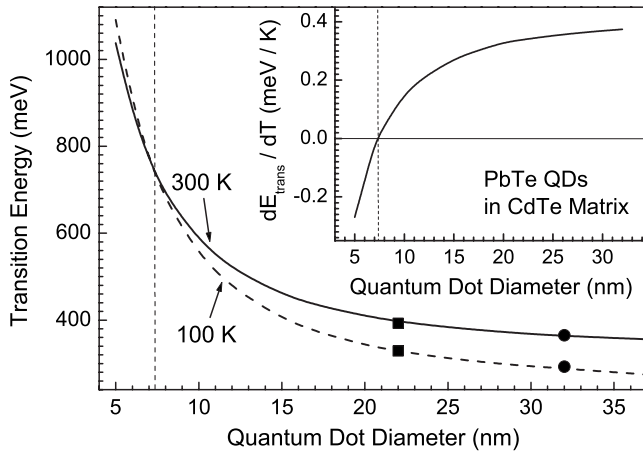


FIG. 5. Calculated ground-state transition energy for spherical PbTe/CdTe quantum dots as a function of the dot diameter for 300 (full line) and 100 K (dashed line). The symbols are the experimental results for the PL peak for the 3 (squares) and 5 nm samples (circles). The inset shows the calculated change of the transition energy with temperature dE_{trans}/dT in dependence of the dot diameter at 300 K.

and are linearly interpolated for intermediate temperatures. Their influence is not very strong due to the low penetration of the dot wave functions into the barrier materials due to the large barrier potential. As discussed above, the anisotropic masses of PbTe are spherically averaged using $m_{av} = \sqrt[3]{m_t^2 m_l}$, where m_t and m_l are the transverse and longitudinal effective masses, respectively.

Another influence is the band offset in the conduction ΔE_c and valence bands ΔE_v . The band offset ratio $\Delta E_c/\Delta E_v$ is unknown for PbTe/CdTe heterostructures. Also the work functions of PbTe and CdTe give no reliable indication because the values in literature scatter strongly. As a consequence, we evaluated the ground transition for various band offsets and found no significant change in the resulting transition energies. Even strongly asymmetric offset ratios of 1:10 or 10:1 result only in a small change in the transition energy of less than 10 meV compared to the symmetric 1:1 case for dots with diameters of 20 nm. For larger dots the difference is even smaller. Thus, we used for all calculations here a symmetric band offset.

C. Results for the calculated transition energy

Adding up the temperature-dependent ground-state energies of electrons and holes and the band gap for isotropically strained PbTe yields the ground-state transition energy as a function of temperature and dot size. The results are plotted in Fig. 5 as a function of the dot diameter for 300 (full line) and 100 K (dashed line). One clearly sees the typical quantum size effect with an increasing transition energy with decreasing dot size as well as the considerable temperature influence for larger dot sizes. Interestingly, the temperature effect becomes smaller with decreasing dot diameter and even changes sign for very small dots (<8 nm diameter, see dotted vertical line).

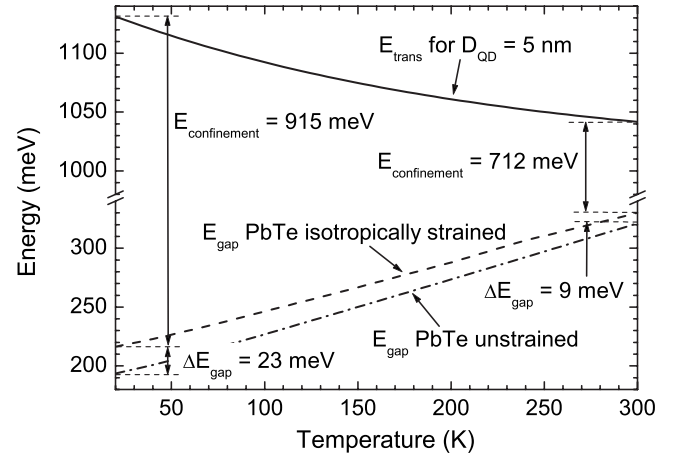


FIG. 6. Calculated ground-state transition energy for a spherical PbTe/CdTe quantum dot with a diameter of 5 nm as a function of temperature (full line). The dashed and dash-dotted lines depict the band gap of isotropically strained PbTe and the band gap of bulklike PbTe, respectively. The confinement energy E_{conf} and the energy change of the band gap of PbTe due to the isotropical strain correction ΔE_{gap} is indicated for 300 and 20 K.

This is shown better in the inset of Fig. 5, depicting the calculated change of the transition energy with temperature dE_{trans}/dT in dependence of the dot size. dE_{trans}/dT is almost independent of temperature (for dots smaller than 10 nm only above 80 K); but with decreasing dot dimensions its value strongly decreases until it is zero and even changes sign for dot diameters below about 8 nm (see dotted vertical line). Also for comparatively large dots (0.39 meV/K for a diameter of 32 nm), it is smaller than the strained bulk band-gap value of $dE_g/dT=0.42$ meV/K because of the still large confinement of about 40 meV. The reason for this effect is the strongly increasing confinement for both electrons and holes with decreasing temperatures due to the decreasing effective masses, which in the case of very small dots even becomes dominant over the strong decrease in the PbTe band gap with decreasing temperature. This surprising observation is illustrated in detail in Fig. 6, showing the calculated transition energy vs temperature for a QD with only 5 nm in diameter together with the strained and bulklike band gaps of PbTe. As indicated in the figure, the large confinement due to the small dot size and small effective masses at low temperatures results indeed in a larger transition energy at lower temperatures (e.g., the confinement energy increases from 712 meV at 300 K to 915 meV at 20 K).

Such an effect was also reported for spherical PbS and PbSe QDs in rigid glass matrices⁵⁵ with dot sizes up to 16 nm in diameter. However, the temperature-dependent confinement due to the temperature-dependent effective masses was not taken into account as a reason for this observation but instead the thermal expansion of the lattice and the electron-phonon coupling.⁵⁵

V. COMPARISON OF THE CALCULATION WITH THE EXPERIMENTAL DATA

Finally, we compare our calculation with the experiments shown in Figs. 1 and 2. The arrows in Fig. 1 are the results of

the calculated ground transition energy for three different dot diameters (D_{QD}). For the 3 nm sample, an average dot size of 22 nm yields the best agreement to the PL peak at all temperatures, whereas for the 5 nm sample a larger average dot diameter of 32 nm is found (see full arrows). One clearly sees that the temperature dependence of the PL emission is very well reproduced by the calculation despite the approximation of the dot shape by a sphere. Moreover, the dot dimensions deduced from the model calculations fit quite well to the dot sizes determined from our recent TEM studies on the PbTe dots,³² which yielded dot diameters of around 20 nm for a sample with a 3 nm PbTe layer. This indicates the reliability of the calculation presented here.

From the calculated transition energies as a function of dot size as shown in Fig. 1 by the dashed and dotted arrows, one is also able to estimate the dot size dispersion and the influence of the average QD size on the transition energy. As can be seen in Fig. 1, the influence of the dot size variation becomes significantly larger with decreasing temperature due to the increasing quantum confinement. If one assumes that the width of the PL peak at the lowest measurement temperature of 20 K directly reflects the size dispersion of the dots (no homogeneous broadening), this dispersion is estimated as $\pm 10\%$ or lower for both dot sizes. Consequently, with rising temperature, due to the decreasing influence of the average dot size on the PL peak position, the linewidth should become narrower by about a factor of 1.5 from 20 to 300 K (see the distance between the arrows in Fig. 1 at each temperature). However, we observe only a small narrowing from 20 to about 120 K and, at higher temperatures, even a broadening of the linewidth. This demonstrates that homogeneous broadening of the PL linewidth with rising temperature is a considerable effect. A strong homogeneous broadening attributed to enhanced coupling to acoustic phonons was also observed for small, strongly confined colloidal PbS nanocrystals.⁵⁶

The good agreement of the calculation with the temperature dependence of the PL peak is also seen in Fig. 2, in which the full line depicts the calculated ground transition energy for the two dot sizes of 22 [Fig. 2(a)] and 32 nm [Fig. 2(b)] as a function of temperature. Evidently, the data points of the PL peak energy fit very well to the calculation for both dot sizes. Only at lower temperatures (< 100 K), a slight deviation to lower energies on the order of a few percent is observed. This is attributed to thermal carrier redistribution to energetically favorable larger dots, as outlined in Sec. III B. By comparing the data to the calculated band gap of isotropically strained PbTe (dashed lines in Fig. 2), one again sees the different contributions to the transition energy, i.e.,

the band gap of bulk PbTe (dash-dotted lines), the strain in the dot, and the confinement changing with temperature due to the temperature dependence of both the lattice mismatch between PbTe and CdTe and the effective masses of PbTe. The experimental PL peak positions for the two dot sizes of 22 (squares) and 32 nm (circles) for 300 and 100 K are also plotted into Fig. 5 for comparison to the calculated data, again showing the good agreement.

VI. CONCLUSION

To summarize, we presented the temperature dependence of continuous-wave midinfrared photoluminescence of PbTe quantum dots in a CdTe matrix for two different dot sizes. These QDs are formed by epitaxial precipitation of an initially continuous PbTe layer upon thermal annealing because of the immiscibility of PbTe and CdTe. A strong shift of the single PL peak to longer wavelengths with decreasing temperature was found for both dot sizes. This shift is not just explained by the strong temperature dependence of the band gap of PbTe but also by the strain in the dots as well as by the change in the quantization energies with temperature due to the changing lattice mismatch between PbTe and CdTe, and the effective masses of PbTe.

We also observed an increase in the PL intensity with rising temperature before it starts to decrease above a certain temperature due to thermally activated carrier evaporation out of the dots. The temperature with the maximum PL output is between 50 and 100 K, depending on the size of the dots. We attributed this behavior to a splitting of the ground state into a bright state and a dark state lying below the bright state, as was also proposed for other quantum dots. In addition, the influence of the excitation power on the PL spectra at various temperatures was analyzed, indicating carrier redistribution between the dots.

Furthermore, a calculation of the ground-state transition energy responsible for the PL emission was presented. For this analytical calculation, we made use of the fact that the ground-state transition in a spherical dot with finite barrier heights can be calculated in analogy to the first-excited state in a quantum well with the same dimensions. We also included the temperature-dependent strain in the dots and the matrix as well as the temperature-dependent effective masses of PbTe. In that way, a good agreement to the experimental data was obtained over the whole temperature range from 300 to 20 K.

ACKNOWLEDGMENTS

The authors thank T. Fromherz and M. Simma for helpful discussions concerning the calculations. This work was supported by the FWF, Vienna.

*Corresponding author; thomas.schwarzl@jku.at

¹M. Grundmann *et al.*, Phys. Rev. Lett. **74**, 4043 (1995).

²L. Landin, M. S. Miller, M. E. Pistol, C. E. Pryor, and L. Samuelson, Science **280**, 262 (1998).

³S. Fafard, R. Leon, D. Leonard, J. L. Merz, and P. M. Petroff,

Phys. Rev. B **50**, 8086 (1994).

⁴Z. I. Alferov, in *Nano-Optoelectronics*, edited by M. Grundmann (Springer, Berlin, 2002), pp. 3–22.

⁵G. T. Liu, A. Stintz, H. Li, K. J. Malloy, and L. F. Lester, Electron. Lett. **35**, 1163 (1999).

- ⁶G. Park, O. B. Shchekin, S. Csutak, D. L. Huffaker, and D. G. Deppe, *Appl. Phys. Lett.* **75**, 3267 (1999).
- ⁷S. Fafard, K. Hinzer, S. Raymond, M. Dion, J. McCaffrey, Y. Feng, and S. Charbonneau, *Science* **274**, 1350 (1996).
- ⁸D. Leonard, M. Krishnamurthy, C. M. Reeves, S. P. Denbaars, and P. M. Petroff, *Appl. Phys. Lett.* **63**, 3203 (1993).
- ⁹S. Sanguinetti, M. Henini, M. Grassi Alessi, M. Capizzi, P. Frigeri, and S. Franchi, *Phys. Rev. B* **60**, 8276 (1999).
- ¹⁰E. C. Le Ru, J. Fack, and R. Murray, *Phys. Rev. B* **67**, 245318 (2003).
- ¹¹L. Brusaferrri *et al.*, *Appl. Phys. Lett.* **69**, 3354 (1996).
- ¹²T. Mano, K. Watanabe, S. Tsukamoto, N. Koguchi, H. Fujioka, M. Oshima, C.-D. Lee, J.-Y. Leem, H. J. Lee, and S. K. Noh, *Appl. Phys. Lett.* **76**, 3543 (2000).
- ¹³S. Sanguinetti, T. Mano, M. Oshima, T. Tateno, M. Wakaki, and N. Koguchi, *Appl. Phys. Lett.* **81**, 3067 (2002).
- ¹⁴V. Tasco, N. Deguffroy, A. N. Baranov, E. Tournié, B. Satpati, A. Trampert, M. S. Dunaevskii, and A. Titkov, *Appl. Phys. Lett.* **89**, 263118 (2006).
- ¹⁵G. Bauer, M. Kriechbaum, Z. Shi, and M. Tacke, *J. Nonlinear Opt. Phys. Mater.* **4**, 283 (1995).
- ¹⁶T. Schwarzl, G. Springholz, M. Böberl, E. Kaufmann, J. Roither, W. Heiss, J. Fürst, and H. Pascher, *Appl. Phys. Lett.* **86**, 031102 (2005).
- ¹⁷M. Tacke, *Infrared Phys. Technol.* **36**, 447 (1995).
- ¹⁸M. Böberl, T. Fromherz, J. Roither, G. Pillwein, G. Springholz, and W. Heiss, *Appl. Phys. Lett.* **88**, 041105 (2006).
- ¹⁹P. C. Findlay *et al.*, *Phys. Rev. B* **58**, 12908 (1998).
- ²⁰G. Nimtz, in *Numerical Data and Functional Relationships in Science and Technology*, Landolt-Börnstein, New Series, Group III, Vol. 17, Pt. F, edited by O. Madelung, M. Schulz, and H. Weiss (Springer, Berlin, 1983), pp. 162–179.
- ²¹H. Preier, *Appl. Phys.* **20**, 189 (1979).
- ²²J. Pietryga, R. Schaller, D. Werder, M. Stewart, V. Klimov, and J. Hollingsworth, *J. Am. Chem. Soc.* **126**, 11752 (2004).
- ²³B. Wehrenberg, C. Wang, and P. Guyot-Sionnest, *J. Phys. Chem. B* **106**, 10634 (2002).
- ²⁴M. Kovalenko, E. Kaufmann, D. Pachinger, J. Roither, M. Huber, J. Stangl, G. Hesser, F. Schaffler, and W. Heiss, *J. Am. Chem. Soc.* **128**, 3516 (2006).
- ²⁵G. Springholz, V. Holy, M. Pinczolit, and G. Bauer, *Science* **282**, 734 (1998).
- ²⁶G. Springholz, M. Pinczolit, P. Mayer, V. Holy, G. Bauer, H. H. Kang, and L. Salamanca-Riba, *Phys. Rev. Lett.* **84**, 4669 (2000).
- ²⁷M. Simma, T. Fromherz, A. Raab, G. Springholz, and G. Bauer, *Appl. Phys. Lett.* **88**, 201105 (2006).
- ²⁸W. Heiss, H. Groiss, E. Kaufmann, G. Hesser, M. Böberl, G. Springholz, F. Schaffler, K. Koike, H. Harada, and M. Yano, *Appl. Phys. Lett.* **88**, 192109 (2006).
- ²⁹W. Heiss *et al.*, *J. Appl. Phys.* **101**, 081723 (2007).
- ³⁰R. Leitsmann, L. E. Ramos, and F. Bechstedt, *Phys. Rev. B* **74**, 085309 (2006).
- ³¹R. Leitsmann, L. E. Ramos, F. Bechstedt, H. Groiss, F. Schaffler, W. Heiss, K. Koike, H. Harada, and M. Yano, *New J. Phys.* **8**, 317 (2006).
- ³²H. Groiss *et al.*, *Appl. Phys. Lett.* **91**, 222106 (2007).
- ³³S. Yuan, H. Krenn, G. Springholz, Y. Ueta, G. Bauer, and P. J. McCann, *Phys. Rev. B* **55**, 4607 (1997).
- ³⁴G. Nimtz, in *Numerical Data and Functional Relationships in Science and Technology*, Landolt-Börnstein, New Series, Group III, Vol. 17, Pt. B, edited by O. Madelung, M. Schulz, and H. Weiss (Springer, Berlin, 1982), pp. 225–230.
- ³⁵V. Leute and R. Schmidt, *Z. Phys. Chem.* **172**, 81 (1991).
- ³⁶K. Koike, T. Itakura, T. Hotei, and M. Yano, *Appl. Phys. Lett.* **91**, 181911 (2007).
- ³⁷K. Koike, H. Harada, T. Itakura, M. Yano, W. Heiss, H. Groiss, E. Kaufmann, G. Hesser, and F. Schaffler, *J. Cryst. Growth* **301–302**, 722 (2007).
- ³⁸L. I. Schiff, *Quantum Mechanics* (McGraw-Hill, Tokyo, 1955).
- ³⁹K. Koike, T. Tanaka, S. Li, and M. Yano, *J. Cryst. Growth* **227–228**, 671 (2001).
- ⁴⁰K. Koike, T. Honden, I. Makabe, F. P. Yan, and M. Yano, *J. Cryst. Growth* **257**, 212 (2003).
- ⁴¹K.-S. Cho, D. Talapin, W. Gaschler, and C. Murray, *J. Am. Chem. Soc.* **127**, 7140 (2005).
- ⁴²S.-H. Wei and A. Zunger, *Phys. Rev. B* **55**, 13605 (1997).
- ⁴³R. Espiau de Lamaestre, H. Bernas, D. Pacifici, G. Franzó, and F. Priolo, *Appl. Phys. Lett.* **88**, 181115 (2006).
- ⁴⁴J. An, A. Franceschetti, and A. Zunger, *Nano Lett.* **7**, 2129 (2007).
- ⁴⁵Z. Y. Xu, Z. D. Lu, X. P. Yang, Z. L. Yuan, B. Z. Zheng, J. Z. Xu, W. K. Ge, Y. Wang, J. Wang, and L. L. Chang, *Phys. Rev. B* **54**, 11528 (1996).
- ⁴⁶S. Mackowski, G. Pechtl, W. Heiss, F. V. Kyrychenko, G. Karczewski, and J. Kossut, *Phys. Rev. B* **69**, 205325 (2004).
- ⁴⁷T. N. Xu, H. Z. Wu, J. X. Si, and P. J. McCann, *Phys. Rev. B* **76**, 155328 (2007).
- ⁴⁸G. E. Tudury, M. V. Marquezini, L. G. Ferreira, L. C. Barbosa, and C. L. Cesar, *Phys. Rev. B* **62**, 7357 (2000).
- ⁴⁹D. Bimberg, M. Grundmann, and N. Ledentsov, *Quantum Dot Heterostructures* (Wiley, Berlin, 1999).
- ⁵⁰J. P. Hirth and J. Lothe, *Theory of Dislocations* (McGraw-Hill, New York, 1968).
- ⁵¹B. Houston, R. E. Strakna, and H. S. Belson, *J. Appl. Phys.* **39**, 3913 (1968).
- ⁵²R. D. Greenough and S. B. Palmer, *J. Phys. D* **6**, 587 (1973).
- ⁵³J. S. Browder and S. S. Ballard, *Appl. Opt.* **11**, 841 (1972).
- ⁵⁴G. Harbecke, O. Madelung, and U. Rössler, in *Numerical Data and Functional Relationships in Science and Technology*, Landolt-Börnstein, New Series, Group III, Vol. 17, Pt. A, edited by O. Madelung, M. Schulz, and H. Weiss (Springer, Berlin, 1982), pp. 218–258.
- ⁵⁵A. Olkhovets, R.-C. Hsu, A. Lipovskii, and F. W. Wise, *Phys. Rev. Lett.* **81**, 3539 (1998).
- ⁵⁶M. Fernee, P. Jensen, and H. Rubinsztein-Dunlop, *J. Phys. Chem. C* **111**, 4984 (2007).